JOURNAL OF PROPULSION AND POWER
Vol. 23, No. 1, January–February 2007

Simple Numerical Modeling for Gasdynamic Design of Wave Rotors

Koji Okamoto* and Toshio Nagashima†
University of Tokyo, Tokyo 113-8656, Japan

DOI: 10.2514/1.18470

The estimation of pressure waves generated in the cells or rotor passages is a crucial factor in wave rotor design. However, it is difficult to estimate the pressure wave analytically, for example, by the method of characteristics, because the mechanism of pressure wave generation and propagation in the cells is extremely complicated as compared with that in a shock tube. In this study, a simple numerical modeling scheme was developed to facilitate the design procedure. This scheme considers three dominant factors in the loss mechanism (gradual passage opening, wall friction, and leakage) for simulating the pressure waves precisely. The numerical scheme itself is based on the one-dimensional Euler equations with appropriate source terms to reduce the calculation time. The modeling of these factors was verified by comparing the results with those of a two-dimensional numerical simulation; the results were validated by the experimental data in our previous study. With regard to wave rotor miniaturization, the leakage flow effect that involves the interaction between adjacent cells was investigated extensively. A port configuration principle was also examined and analyzed in detail to verify the applicability of the present numerical modeling scheme to the wave rotor design.

Nomenclature

a	=	sound speed
D_h	=	hydraulic diameter of a wave rotor channel
e	=	total energy
L	=	cell length
p	=	static pressure
p_0	=	total pressure
r	=	mean rotor radius
t	=	time
u	=	velocity
U	=	velocity of the main stream in a channel
W_{cell}	=	cell width
x	=	position in axial direction
μ	=	viscous coefficient
ν	=	kinetic viscosity
ρ	=	density
τ	=	nondimensional parameter for the gradual passage opening effect
τ_{wall}	=	wall shear stress
ω	=	angular speed of the rotor, rad/s

Introduction

THE total pressure ratio and turbine inlet temperature primarily determine the performance of a gas turbine. The performance can be enhanced by topping the gas turbine with a wave rotor [1–3]. Figure 1 shows the wave rotor topped gas turbine and its temperature–entropy diagram. The wave rotor has an advantage over conventional impellers in terms of the heat resistance and compression ratio. Therefore, the maximum temperature and total pressure ratio can be increased dramatically to facilitate the increase in pressure at the turbine inlet.

Received 28 June 2005; revision received 10 June 2006; accepted for publication 24 June 2006.

*Research Associate, Department of Aeronautics and Astronautics, 7-3-1, Hongo, Bunkyo-ku.

†Professor, Department of Aeronautics and Astronautics, 7-3-1, Hongo, Bunkyo-ku.

Figure 2 shows a wave diagram that schematically represents the flow and pressure wave dynamics of the entire wave rotor cycle in the form of characteristic lines. This wave diagram corresponds to the four-port through flow type of wave rotor cycle; this is one of the candidates to be topped on the gas turbine cycle. In this type of wave rotor, hot combustion gas and cold fresh air flow through the cells or rotor passages alternately. Therefore, the rotor cools itself such that a higher combustion gas temperature is attained without using bleed air, which is advantageous to the entire cycle performance, as compared with the conventional turbomachinery. The compression is achieved by shock waves and the pressure ratio across the shock wave is greater than two; this enables the compression to be achieved within the shortest distance.

As shown in Fig. 2, each port should be designed to open and close the cells with precise timing according to the pressure wave motion. Therefore, it is essential to precisely simulate the propagation velocity of the pressure waves. However, this is extremely difficult because the internal flow dynamics are significantly different from those in an ordinary shock tube. In the previous research [4–8], 2-D and 3-D numerical simulations satisfactorily predicted the pressure waves and fluid motion; however, the cost involved in performing these simulations was extremely high and, therefore, they were not employed in the design phase. Hence, in this study, a simple 1-D numerical modeling scheme was developed for the simulations in the wave rotor design process [9]. Its accuracy was verified by comparing the results with those obtained by a more precise 2-D numerical simulation.

It is noteworthy that micro gas turbines (MGT) have become popular among the distributed electricity generation systems, and the recent trend is toward miniaturized systems such as ultra micro gas turbine (UMGT) [10–12] and power-MEMS turbine [13] that employ micromachining or advanced micro-electro-mechanical system (MEMS) fabrication technology. One of the key issues in the development of such miniaturized turbomachinery is to avoid the reduction in efficiency due to extremely narrow flow passages. Another issue is the difficulty in achieving a high cycle performance due to the temperature limitation on the material. Power-MEMS turbine [13], for example, has the maximum temperature below 1600 K for SiC: a candidate MEMS material. It is also extremely difficult to maintain a high thermocycle temperature ratio in such small devices, because the heat convection transfer will be very low compared with the material conduction; therefore, the temperature easily becomes uniform within the material of the entire device. Under such circumstances, a wave rotor can offer remarkable

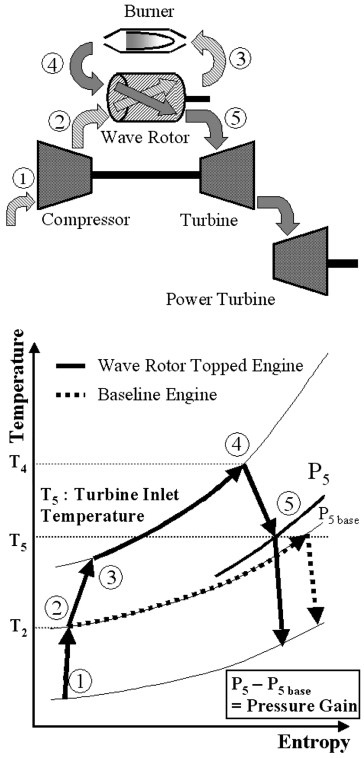

Fig. 1 Wave rotor topped gas turbine.

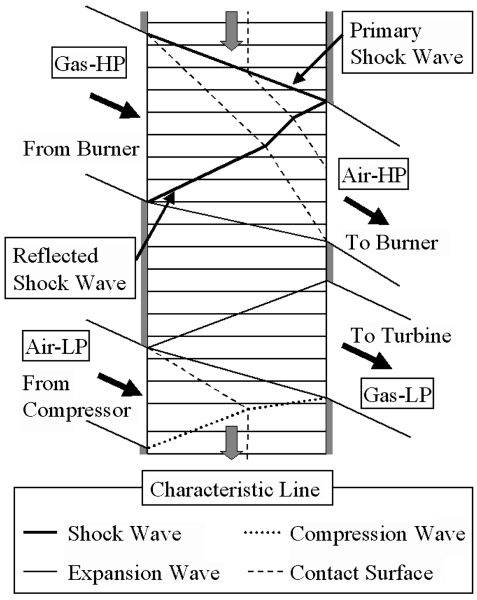

Fig. 2 Wave diagram.

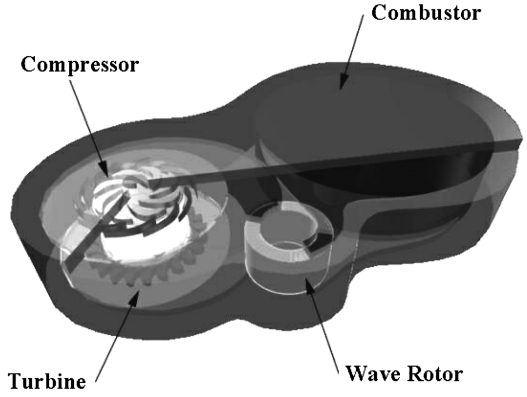

Fig. 3 Wave rotor topped UMGT (concept).

advantages for a topping gas turbine cycle [1,2,14], because its unsteady flow process differs significantly from the blade mechanics when the passages become narrower; this is due to the nature of the wave dynamics. Furthermore, by placing the wave rotor such that the turbine rotor is separated from the combustor, it will be possible to raise the combustor temperature independently of the turbine inlet temperature. Such a design choice may be feasible for a combustor that is a less restrictive component than rotating parts and is thus capable of adopting a thermal insulator, cooling system, and fabrication with alternative heat-resistive materials. Figure 3 shows the proposed arrangement for wave rotor integration with the installation of a separate combustor for the UMGT [15].

As mentioned earlier, the research on miniaturized wave rotors is profoundly interesting from the viewpoint of the recent trend towards miniaturization in turbomachinery. However, there is no database presently available for designing such miniaturized wave rotors; hence, there are immediate requirements in the design and practice to bridge the gap between the established macro wave rotor technology and the unexplored miniaturized wave rotor for the UMGT. In this study, a micro wave rotor matched with a MGT of several kilowatt output was designed by employing a developed numerical scheme and relying on the available database of a conventional macro wave rotor [16–18]. Several different configurations of the wave rotor are discussed and compared. This will be the first step to explore the feasibility of using an even smaller ultra micro scale wave rotor to match with the UMGT in the future.

Numerical Modeling Scheme

The numerical modeling scheme for the wave rotor design process must accurately simulate the pressure wave dynamics with a minimum load on the CPU. For this purpose, the cell is treated as a 1-D tube, as described in previous studies [19–22]. The flow is assumed to be inviscid, adiabatic, and compressible, with the perfect gas having constant specific heats, whereas the wall friction effect is taken into account by introducing unsteady shear force. This treatment implies that the internal flow dynamics are almost 1-D, which is similar to those in a shock tube. Therefore, the interaction of a propagating shock wave with the viscous layer along the tube wall and certain complicated flow structures, such as those resulting from the interface between the gas and air and the effect of centrifugal forces, had to be neglected. The propagation velocity of the shock waves in a wave rotor differs significantly from that in a shock tube at the same pressure ratio, as described in the authors' previous study [4]. Therefore, additional treatments are required to simulate the pressure waves accurately.

There are several dominant factors responsible for the performance loss; the following three factors were considered in the present modeling: 1) gradual passage opening, 2) leakage flow, and 3) wall friction.

According to the previous experimental studies [23,24], these factors are considered to be very important. It is necessary to develop a model for each factor, because they cannot be determined by 1-D treatment without the appropriate assumptions.

Governing Equations and Solution Scheme

The present simulation of the pressure waves within a cell is based on the governing equations of the 1-D Euler formulation with a source term as shown next.

$$\frac{\partial}{\partial t}\begin{bmatrix}\rho\\ \rho u\\ e\end{bmatrix}+\frac{\partial}{\partial x}\begin{bmatrix}\rho u\\ \rho u^2+p\\ (e+p)u\end{bmatrix}=\begin{bmatrix}0\\ S_2\\ 0\end{bmatrix} \tag{1}$$

The source term S_2 on the right indicates the momentum loss due to wall friction, which will be explained later. In this case, the mixture

loss at the contact surface of gas and air was assumed to be negligible. The source term in the mass conservation equation is zero, because it is applicable only to the cell region in which there is no leakage. In other words, the leakage flow occurs only at the interface between the cells and the ports. The source term in the energy equation is also zero, because the wall was assumed to be adiabatic in this equation. The modeling that takes the diabatic process into account will be undertaken in the future; it should be noted that heat transfer will have a substantial influence on the inner flow dynamics, especially in the miniaturized wave rotors due to the increased surface over volume ratio.

For the numerical scheme, the convective terms were solved by the finite difference method (FDM) by incorporating Chakravarthy–Osher's third-order upwind TVD scheme with van Leer's differentiable limiter [25,26]. Jameson–Baker's four-stage Runge–Kutta scheme (fourth-order accurate) was employed for time integration [27]. These treatments are identical to those adopted in the 2-D numerical simulation [4], whose results were used for verifying the numerical modeling in the present study.

Gradual Passage Opening Effect

This effect is due to the relative rotation process in which the cells are gradually opened and closed to the ports, which significantly influences the pressure wave generation. Figure 4 illustrates the interface between a cell and a port at the left end when the cell begins to open to the port. The volume of the clearance region is divided into A and B. Volume B is exposed to the port, and volume A is exposed to the end wall. Volume C belongs to the port, which is assumed to be uniform and constant throughout the calculation. The relative inflow and outflow angles to the cells are assumed to be always zero, which implies an ideally smooth inflow and outflow without loss at the cell–port interface. Volume D corresponds to the boundary volume in the calculation using Eq. (1), because only the cell region is calculated by the present CFD approach. To determine the condition of volume D in the next time step, the fluxes between the surrounding volumes (A, B, and D') were calculated at every time step by using the exact Riemann solver [28]. In addition, the conditions for volumes A and B are determined in the same manner by calculating the flux in the axial, circumferential, and radial direction. The fluxes considered in the axial and circumferential directions are shown in Fig. 4, and the flux in the radial direction is considered for the leakage effect, which is mentioned in the next section. The numerical treatment for estimating the flux is the same as those adopted in the 2-D simulation in the previous paper [4], although the shear stress at each interface was not considered. The problem in this modeling of the gradual passage opening effect was how to set the initial condition of volume A at each time step. Therefore, three different treatments were tested and compared, which will be mentioned later.

Leakage Flow Effect

The leakage flow during the operation of the wave rotor indicates the radial as well as circumferential flows in the clearance region between the rotor and the end wall that is subdivided into volumes A, B, and G, as shown in Fig. 4. The horizontal length of these volumes is equivalent to the clearance gap; therefore, volume D, which is allocated at the end of the cell, has a horizontal length equal to the clearance gap when the leakage flow effect is taken into account. For modeling, the leakage flow was considered to comprise two components: the flow in the radial direction toward the outside and that in the circumferential direction due to the interaction between the neighboring cells.

To determine the leakage flow to the outside, the flux in the radial direction was calculated for volumes A, B, and G, taking into account the cell height of these volumes. The external condition used for calculating the flux of the radial leakage flow was assumed to be constant and the same as the stagnation condition in the air low pressure port (Air-LP), whereas the interaction between the neighboring cells was determined by considering the flux between volumes A and G. It should be noted that when a cell is completely

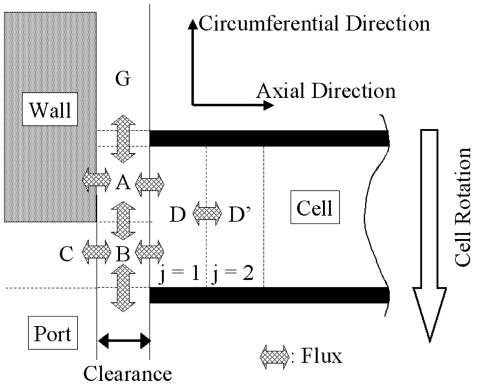

Fig. 4 Modeling of gradual passage opening and leak flow effects

opened or closed to the port, the clearance region is no longer divided into volumes A and B. However, the fluxes in both the radial and circumferential directions should be considered.

Friction Effect

In the current modeling, only the momentum loss due to the shear stress on the walls was considered for the friction effect. Therefore, the source term S_2 in the 1-D governing Eq. (1) was calculated, as shown next.

$$S_2 = -4\frac{\tau_{\text{wall}}}{D_h} \tag{2}$$

Several different expressions for the shear stress have been suggested [20–22]. The boundary layer that is induced on the wall by a shock wave was investigated in relation to shock attenuation and the resulting deviations from the flow properties in a shock tube; wherein the Rayleigh flow problem yielded a good solution to the corresponding laminar boundary-layer growth with zero pressure gradient in the stream behind the propagating shock wave. Although the Rayleigh flow analogy is valid for only a weak shock wave and little is known about the actual flow profiles within the cell cross section, it is better to apply this analogy than to use an empirical friction coefficient based on the flow dynamic pressure, because the latter neglects the unsteady flow nature. Therefore, the present model employs the simplest expression as follows:

$$\tau_{\text{wall}} = \frac{\mu U}{\sqrt{\pi \nu t}}$$

where t is L/a. The viscous coefficient and kinetic viscosity were

Table 1 Equipment design

Cell length	186 mm
Cell height	16 mm
Cell width	8 mm
Rotor mean radius	60 mm
Rotating speed	4200 rpm
Wall thickness between the cells	1.0 mm
Clearance	0.5–1.0 mm (variable)

Table 2 Port conditions (outer region conditions for Riemann solver)

	Gas-HP	Air-HP
Total pressure, MPa	0.26	0.2
Total temperature, K	288	288
Velocity, m/s (axial direction)	160	0.0
Velocity, m/s (circumferential direction)	26.4	0.0
Opening time, deg	0.0	29.0
Closing time, deg	13.0	39.5

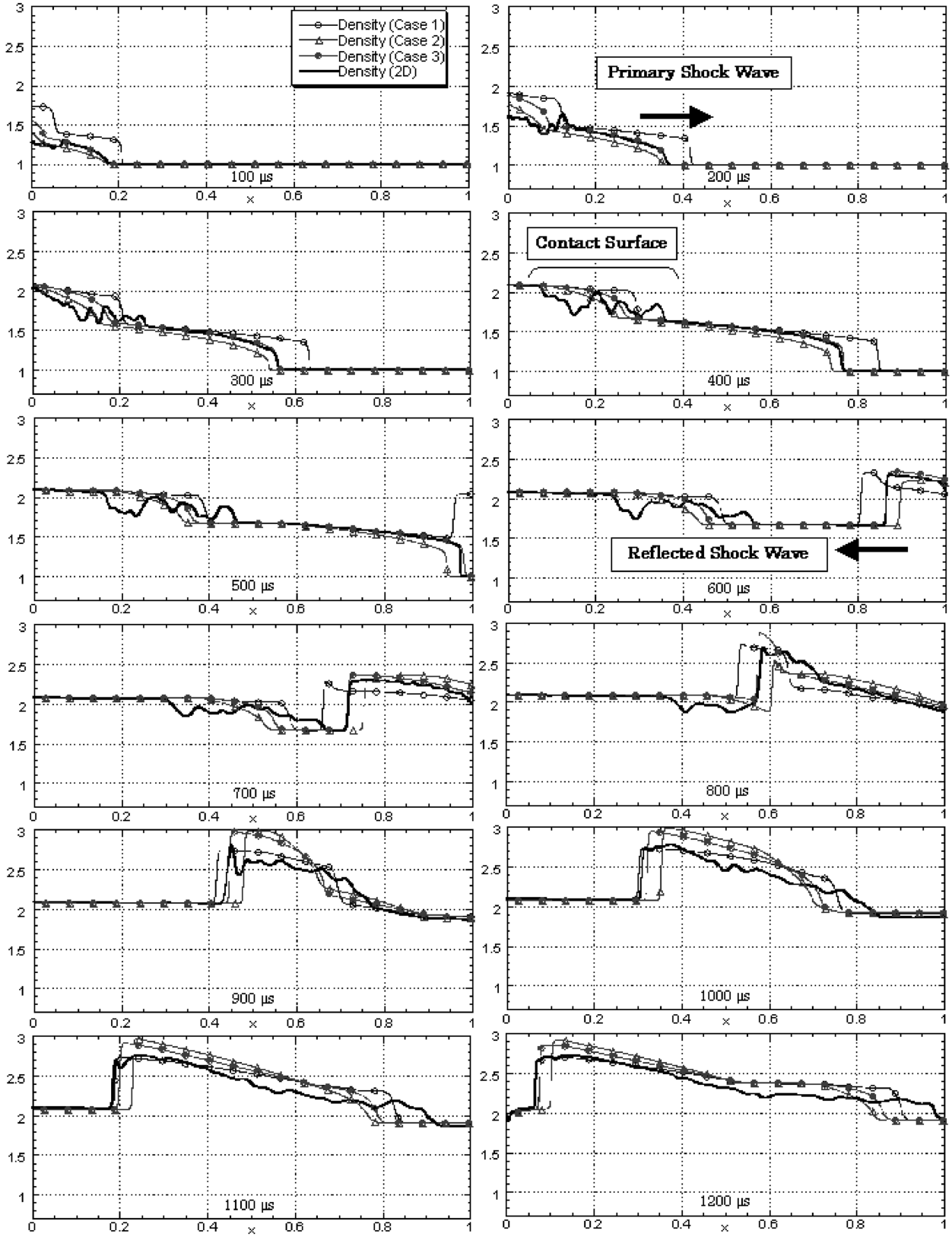

Fig. 5 Validation of modeling for gradual passage opening effect (density distribution normalized by the Air-LP value in the axial direction).

estimated using Sutherland's law, and the turbulent viscosity was not taken into account.

Validation

To validate the numerical modeling scheme, the calculation results were compared with the 2-D numerical simulation results. For the 2-D numerical simulation, the governing equations were the 2-D Navier–Stokes equations with laminar viscosity. To achieve the same numerical treatment, the spatial discretization and time integration schemes for the 1-D numerical simulation used were entirely the same as those for the 2-D numerical simulation. For the comparison, the design specifications and gas conditions of the cells and ports, which

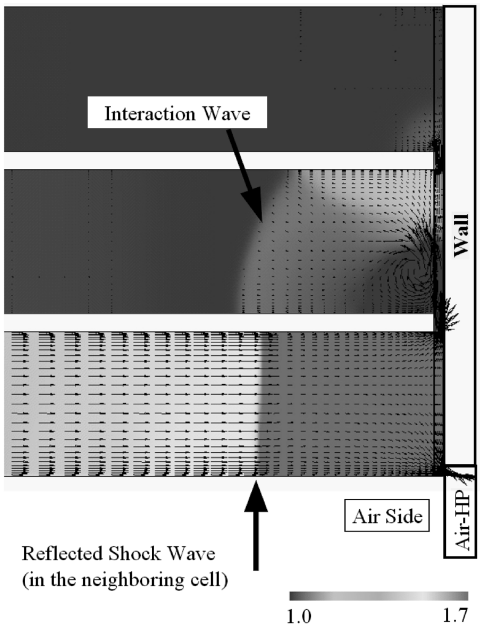

Fig. 6 Interaction wave occurrence [4]: density contour normalized by the Air-LP value (clearance, 0.5 mm; cell width, 8 mm).

were also used in the experiments, are listed in Tables 1 and 2.

Single-Passage Case

First, the results of a single-passage simulation were compared by investigating the treatment of the gradual passage opening effect. This effect has a considerable influence on the generation of primary and reflected shock waves that are responsible for air compression; therefore, the comparison is shown only for the compression process here. The prediction of the propagation velocity of these shock waves is indispensable for designing the ports.

As mentioned in the previous section, the problem in modeling the gradual passage opening effect was how to set a condition for volume A, as shown in Fig. 4. Therefore, the following three assumptions were tested for the comparison.

Assumption 1: The density and static pressure are the same as those in volume B (the flux in the circumferential direction is not considered).

Assumption 2: All the values are calculated based on the flux between adjacent volumes.

Assumption 3: The density and static pressure are the same as those in volume D.

In addition, the leakage flow or the interaction effect between the neighboring cells has not been considered for the comparison, in order to discuss only the modeling of the gradual passage opening effect. With regard to the spatial resolution in the axial direction of the cell, the grid distribution chosen was the same as that for the 2-D simulation.

Figure 5 shows the results of the density distribution along the axial direction in a cell. In this figure, the density is normalized by the condition of low pressure air, and the abscissa axis is normalized by the cell length. Position $x = 0$ corresponds to the left end of the cell, which is opened to the gas high pressure port (Gas-HP), and $x = 1$ corresponds to the right end of the cell, which is opened to the air high pressure port (Air-HP). The results denoted by 2-D, which form the reference curve, are based on the average value at each cross section.

The following results were obtained from the comparison. For Assumption 1, the propagation velocity of the primary shock wave was estimated to be very high, although the arrival time of the reflected shock wave at the left end was satisfactory. For Assumption 2, the velocities of these two shock waves were estimated to be very low. Assumption 3 holds true for both the shock waves, although a small difference is observed behind the reflected shock wave due to the interaction between the shock wave and the contact surface. Based on a similar examination of the distributions of other conservative values (momentum and total energy), which have not been shown, it was concluded that Assumption 3 is the most suitable for modeling the gradual passage opening effect.

According to the experimental investigation of performance loss mechanisms [24], the gradual passage opening effect can be explained by considering the ratio of the passage opening time to the wave travel time:

$$\tau = \frac{(\text{passage opening time})}{(\text{wave travel time})} = \left(\frac{W_{\text{cell}}}{r\omega}\right) \Big/ \left(\frac{L}{a}\right)$$

Evidently, τ becomes zero in the case of the shock tube. A high value of τ indicates that the influence of the gradual passage opening effect is large. For the design specifications listed in Table 1, τ is calculated to be 0.554, whereas it is typically below 0.5 for the other wave rotors [24]. Therefore, the previously mentioned comparison was performed with a faster rotating speed, which yields a smaller τ value, and the result corresponding to Assumption 3 was verified to show a better agreement. It was observed that a smaller τ value produces flow dynamics that are similar to those in the shock tube. Therefore, the proposed numerical model also yields a good accuracy for other wave rotors, thereby confirming its applicability to the wave rotor design.

Multipassage Case

Next, the results of a multipassage simulation were compared with respect to the leakage flow effect. In this simulation, each cell had 372 grid points in the axial direction, in which the length of the grid interval at the end of the cell was equal to the clearance gap, that is, 0.5 mm. In this case, three cells were considered simultaneously, because it was already confirmed in the 2-D numerical simulation that the three cell passages are sufficient for investigating the interaction effect between the neighboring cells [4]. A striking feature of the interaction was the pressure wave generation due to the reflection of the primary shock wave in the neighboring cell (Fig. 6).

Figure 7 shows a comparison of the normalized density distributions in the middle cell. In this case, the counting of time starts from the moment when the bottom cell was opened to the Gas-HP; therefore, the middle cell is opened to the Gas-HP after 341 μs.

The increase in the pressure of the primary shock wave appeared significantly less steep as compared with that in the single-passage simulation. This is because the gas flows into the middle cell through the clearance region before it is opened to the Gas-HP. The 1-D simulation results hold true for this observation, as shown in Fig. 7. The results also hold true for the reflected shock wave, although a difference was observed after the interaction between the shock wave and contact surface, as in the case of single-passage simulation. Furthermore, the interaction wave appeared in the 1-D simulation results and its wave front was observed to be satisfactory, although its strength was rather weak as compared with that in the 2-D results. This difference was due to a vortex at the end of the air side (Fig. 6). The shear stress in the circumferential direction exerts a significant influence on the generation of the interaction wave. However, it cannot be considered by the 1-D numerical model in which the interaction wave is associated only with the increase in the static pressure. Although there was a slight difference between the 1-D and 2-D simulation results as compared with that of the single-passage simulation, it was concluded that the 1-D numerical modeling scheme could successfully simulate the generation and propagation of the pressure waves, including the interaction wave in the multipassage simulation.

Design of Micro Wave Rotor

The developed 1-D numerical modeling scheme was employed for designing a micro wave rotor for a MGT that can generate power in the kilowatt range. The design conditions and configuration of the

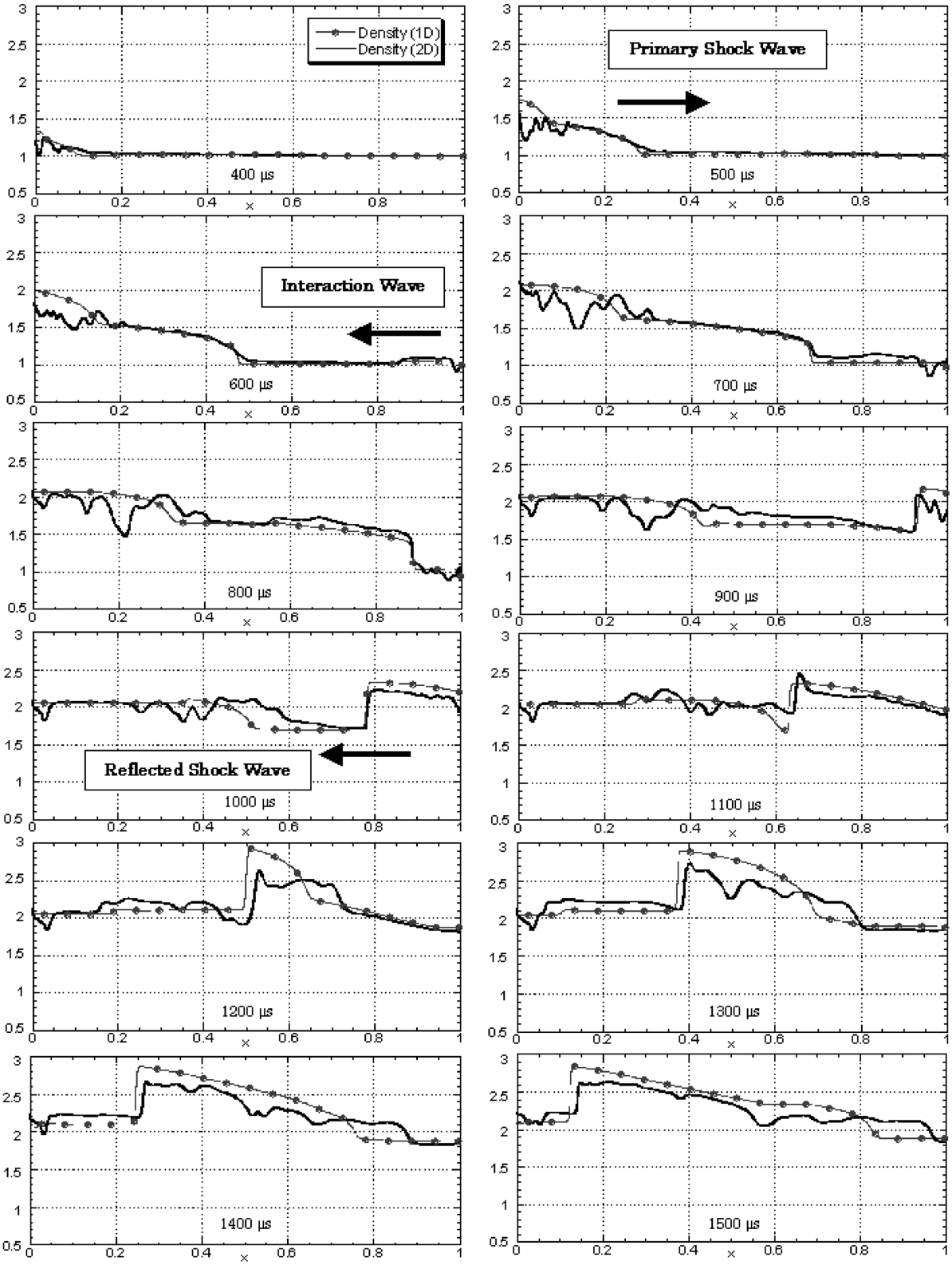

Fig. 7 Validation of modeling for leak flow effect (density distribution normalized by the Air-LP value in the axial direction).

micro wave rotor are listed in Table 3 and Fig. 8, respectively. In this case, the compression ratio of the baseline gas turbine was assumed to be 3.0, the total temperature at the compressor exit was assumed to be 440 K, and the mass flow rate in the Air-LP was assumed to be approximately 20 g/s. The pressure and temperature ratios and the corrected mass flow rate and rotational speed were based on the values in the database, which was developed for a small turboshaft engine used in helicopters [16,17].

In the design of micro wave rotors, the dissipation of shock waves might be significant, particularly for the extremely small ultra micro size that cannot be estimated by using the present 1-D model. It must be noted that the flow structure in wave rotors is different from that in a supersonic duct or a conventional shock tube, because the design factor related to the shock travel time is also important for the boundary-layer formation. The dissipation of shock waves depends on both the length and the cross-sectional area of the cells, which

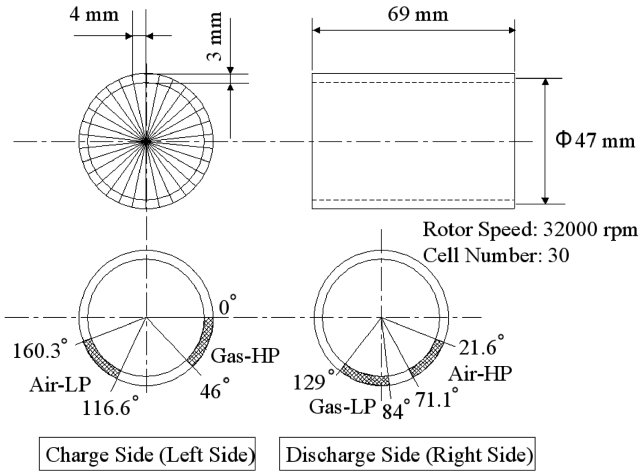

Fig. 8 Design configuration of micro wave rotor.

have to be consulted with the design parameters of wave rotors. The effect of wall friction can be discussed approximately with the parameter L/D_h, according to the parametric study [24]. The value of this parameter for the present micro wave rotor is 20.1, whereas it is around 10–60 in the other wave rotor configurations used in the previous studies [4,24]. Therefore, the dissipation effect was not taken into account in the present work, although this problem in the ultra micro wave rotor will be treated in the future.

Figure 9 shows the distribution of the normalized total temperature that corresponds to the wave diagram. In this figure, the horizontal axis shows the axial position in the cells, the vertical axis shows the circumferential position or cycle time, and the cells are moving downward. The contour indicates the distribution normalized by the stagnation temperature in the Air-LP. The number of grid points used was 601 in the case of a 0.1 mm clearance and 301 in the case of a 0.2 mm clearance for each cell in the axial direction, in which the interval between the grid points at the end of the cells was equal to the clearance gap. In this simulation, the rotor was rotated several times in order to achieve convergence, because the conditions in the cell were not uniform at any circumferential position. The figure corresponds to the total temperature distribution after the fifth rotation in which the convergence was achieved. The results exhibit the same pressure dynamics of the wave diagram shown in Fig. 2. It

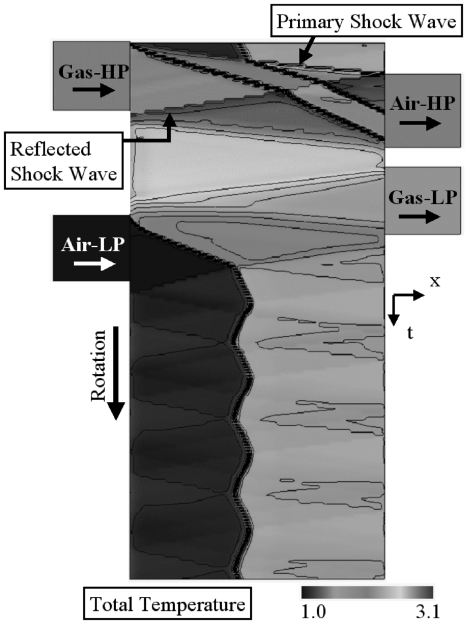

Fig. 9 Micro wave rotor (total temperature contour normalized by the Air-LP value).

Table 3 Port conditions of micro wave rotor

	Gas-HP	Air-LP	Air-HP	Gas-LP
P_0, MPa	0.93	0.30	1.02	0.37
T_0, K	1248	440	907	973

Table 4 Port configurations

	Case 1	Case 2
Gas-HP, deg	0–46	0–46
Air-LP, deg	116.6–160.3	296.1–339.8
Air-HP, deg	21.6–71.1	21.6–71.1
Gas-LP, deg	84–129	263.5–308.5

should be noted that there was a change in the propagation velocity of the primary shock wave due to the total temperature difference across the contact surface. The primary shock wave arrived at the right end precisely when the cell was opened to the Air-HP. The only difference in this case is that weak pressure waves propagated back and forth even after the compression and expansion processes were completed (bottom part in the figure), thereby causing the contact surface to sway slightly.

Compared with the conventional wave rotor, the effect of leakage flow in the micro wave rotor is expected to have a significant influence on its performance, which is a common observation among most turboengines. It is extremely important to develop a method to mitigate the leakage flow effect and also to minimize the clearance. In this study, two different configurations employing a shorter and a longer separation distance between the Air-HP and the gas low pressure port (Gas-LP) were considered for comparison, as listed in Table 4. Figures 8 and 9 correspond to case 1.

Figure 10 shows the dimensionless total pressure distributions (normalized by the stagnation condition in the Air-LP) for the clearances of 0.0, 0.1, and 0.2 mm corresponding to each configuration in Table 4. It should be noted that the contribution of the wave rotor to the entire cycle performance is attributed to the pressure gain at the Gas-LP that is connected to the turbine. Therefore, the pressure in a cell when it just begins to open to the Gas-LP is a direct measure of the pressure gain in the entire cycle; the corresponding point is indicated by a solid black circle in Fig. 10.

As shown in this figure, the dimensionless total pressure was 2.35 in both the cases when the clearance was 0.0 mm. This indicates that the distance between the Air-HP and Gas-LP has no influence on the performance in the present configuration when the leakage effect is absent. On the other hand, a significant difference in the total pressure values of the two cases was observed when the clearance was increased. For the cases shown in Fig. 10, the total pressure in case 1 for the clearance of 0.2 mm was larger than that in case 2 for the clearance of 0.1 mm.

Table 5 compares the ratio of the leakage flow to the mass flow rate at the Gas-HP. In this case, only qualitative discussions were possible because the surrounding conditions of the rotor were assumed to be constant and identical to the Air-LP stagnation condition for this simulation, although in practice the pressure in the rotor cavity is influenced by the leakage flow. Furthermore, the circulatory flow, which flows outside and then back into the cell, was not considered.

As shown in Table 5, the leakage flow in case 1 with the clearance of 0.2 mm was less than that in case 2 with the clearance of 0.1 mm. This is due to the fact that the fluids in the cells leak mainly from the region between the high pressure and the low pressure ports on either side of the cell. Therefore, a better performance can be achieved with a shorter distance between the Air-HP and Gas-LP. For the design of miniaturized wave rotors, this tendency will be further intensified because of the relative increase in the leakage flow area over the wave rotor cross-sectional area.

Based on the preceding discussion, it was concluded that a higher pressure gain can be achieved with a shorter distance configuration.

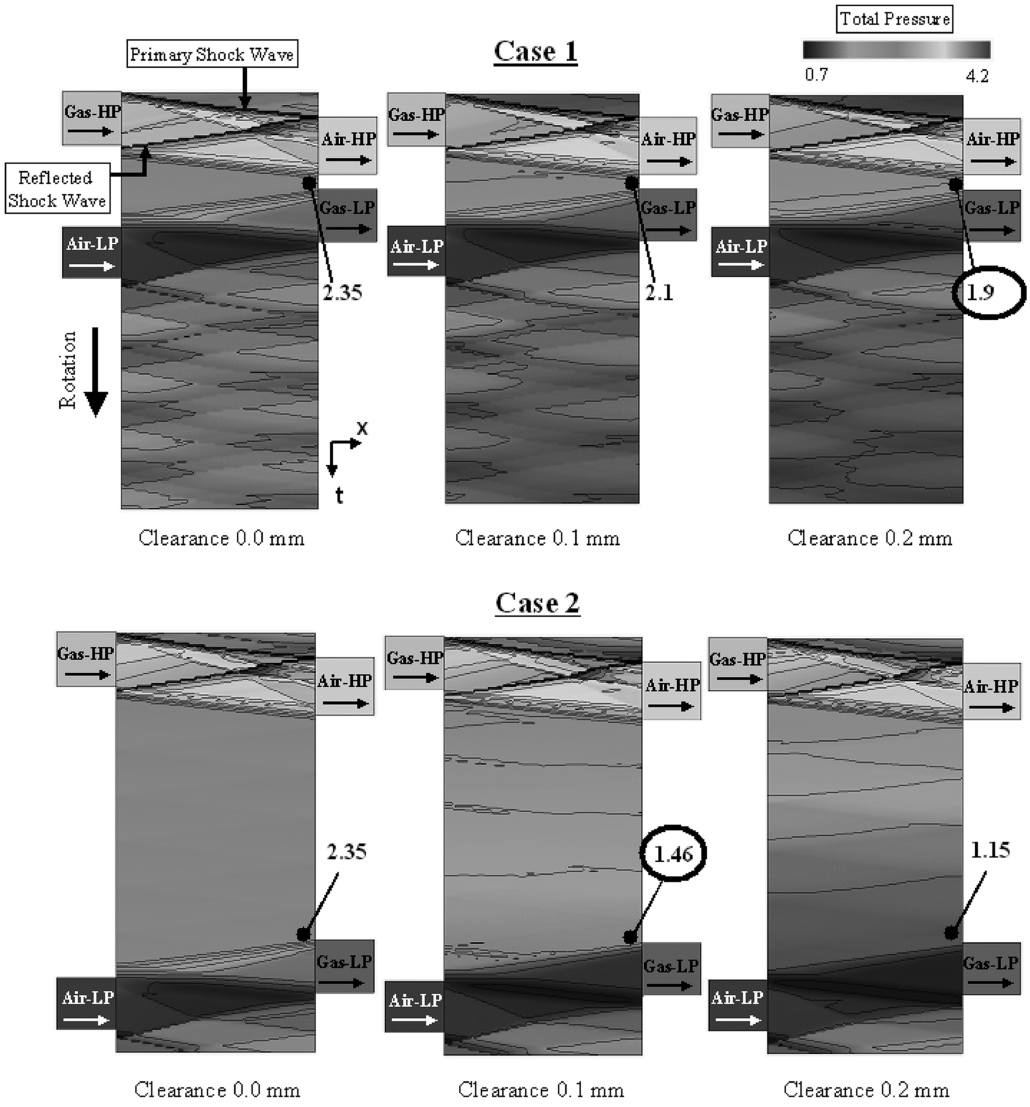

Fig. 10 Comparison of different port configurations (total pressure contour normalized by the Air-LP value).

Therefore, the distance between the Air-HP and Gas-LP must be minimum, that is, approximately equal to the cell width, because the cell should be designed in such a way that it does not open to two ports simultaneously.

Conclusions

A simple numerical modeling scheme for designing a wave rotor was presented. It can simulate the pressure waves generated in the cell passages with minimum load on the CPU. The numerical modeling scheme considered three dominant factors responsible for the performance loss mechanism, gradual passage opening, friction, and leakage flow effects. The computational treatments were verified in detail by comparing the results with those of the 2-D numerical simulation. For the gradual passage opening effect, the best modeling scheme was examined with respect to the numerical flux treatments at the cell end interface in order to accurately simulate the propagation velocity, pressure ratio, and the propagation mechanism of the primary and reflected shock waves. For the leakage effect, the presence of the interaction wave between neighboring cells was simulated and confirmed in addition to the leakage flow to the outside, thereby verifying the present numerical modeling scheme.

By employing the numerical modeling scheme, a micro wave rotor for gas turbines capable of generating power in the kilowatt range was designed based on the database developed for small gas turbines. In such small wave rotors, the performance loss due the leakage flow effect is expected to increase dramatically. In addition to minimizing the clearance, two different port configurations were tested and compared to avoid the leakage loss effect. Based on the comparison, an optimal port design principle was derived wherein the distance between the Air-HP and Gas-LP should be minimum, that is, approximately equal to the cell width.

Table 5 Comparison of leakage mass flow rate

Clearance, mm	Leakage mass flow rate, %	
	Case 1	Case 2
0.0	0.0	0.0
0.1	14.3	26.0
0.2	21.4	35.2

References

[1] Wilson, J., and Paxson, D. E., "Jet Engine Performance Enhancement Through Use of a Wave-Rotor Topping Cycle," NASA TM-4486, 1993.

[2] Welch, G. E., Jones, S. M., and Paxson, D. E., "Wave-Rotor-Enhanced Gas Turbine Engines," *Journal of Engineering for Gas Turbines and Power*, Vol. 119, No. 2, Apr. 1997, pp. 469–477.

[3] Greendyke, R. B., Paxson, D. E., and Schobeiri, M. T., "Dynamic Simulation of a Wave-Rotor-Topped Turboshaft Engine," *Journal of Propulsion and Power*, Vol. 16, No. 5, Sept.–Oct. 2000, pp. 792–796.

[4] Okamoto, K., and Nagashima, T., "Visualization of Wave Rotor Inner Flow Dynamics," *Journal of Propulsion and Power* (submitted for publication).
[5] Welch, G. E., "Two-Dimensional Computational Model for Wave Rotor Flow Dynamics," *Journal of Engineering for Gas Turbines and Power*, Vol. 119, Oct. 1997, pp. 978–985.
[6] Welch, G. E., "Two-Dimensional Numerical Study of Wave Rotor Flow Dynamics," AIAA Paper 93-2525, June 1993.
[7] Larosiliere, L. M., "Wave Rotor Charging Process: Effects of Gradual Opening and Rotation," *Journal of Propulsion and Power*, Vol. 11, No. 1, Jan.–Feb. 1995, pp. 178–184.
[8] Larosiliere, L. M., and Mawid, M., "Analysis of Unsteady Wave Processes in a Rotating Channel," *International Journal for Numerical Methods in Fluids*, Vol. 21, 1995, pp. 467–488.
[9] Okamoto, K., and Nagashima, T., "A Simple Numerical Approach of Micro Wave Rotor Gasdynamic Design," AIAA Paper 2003-1213, 2003.
[10] Nagashima, T., "Lessons Learnt from the Ultra-Micro Gas Turbine Development at University of Tokyo," *Micro Gas Turbines*, RTO-AVT-VKI Lecture Series, von Karman Inst., Sint-Genesius-Rode, Belgium, 2005.
[11] Nagashima, T., Okamoto, K., and Ribaud, Y., "Cycles and Thermal System Integration Issues of Ultra-Micro Gas Turbines," *Micro Gas Turbines*, RTO-AVT-VKI Lecture Series, von Karman Inst., Sint-Genesius-Rode, Belgium, 2005.
[12] Nagashima, T., Kato, C., Teramoto, S., and Yuasa, S., "Aero-thermal Design Particulars in Ultra-Micro Gas Turbines," *Micro Gas Turbines*, RTO-AVT-VKI Lecture Series, von Karman Inst., Sint-Genesius-Rode, Belgium, 2005.
[13] Epstein, A. H., Senturia, S. D., Al-Midani, O., Anathasuresh, G., Ayon, A., Breuer, K., Chen, K.-S., Ehrich, F. F., Esteve, E., and Frechette, L., "Micro-Heat Engines, Gas Turbines, and Rocket Engines," AIAA Paper 97-1773, Jun. 1997.
[14] Fatsis, A., and Ribaud, Y., "Thermodynamic Analysis of Gas Turbines Topped with Wave Rotors," *Aerospace Science and Technology*, No. 5, 1999, pp. 293–299.
[15] Okamoto, K., Nagashima, T., and Yamaguchi, K., "Design and Performance of a Micro Wave Rotor," AIAA Paper 2005-1270, Sep. 2005.
[16] Snyder, P. H., and Fish, R. E., "Assessment of a Wave Rotor Topped Demonstrator Gas Turbine Engine Concept," American Society of Mechanical Engineers Paper 96-GT-41, 1996.
[17] Snyder, P. H., "Wave Rotor Demonstrator Engine Assessment," NASA CR198496, 1996.
[18] Welch, G. E., Paxson, D. E., Wilson, J., and Snyder, P. H., "Wave-Rotor-Enhanced Gas Turbine Engine Demonstrator," NASA TM-1999-209459, 1999.
[19] Paxson, D. E., "A General Numerical Model for Wave Rotor Analysis," NASA, TM-105740, 1992.
[20] Paxson, D. E., and Wilson, J., "An Improved Numerical Model for Wave Rotor Design and Analysis," AIAA Paper 93-0482, Jan. 1993.
[21] Paxson, D. E., and Wilson, J., "Recent Improvements to and Validation of the One Dimensional NASA Wave Rotor Model," NASA, TM-106913, May 1995.
[22] Fatsis, A., Lafond, A., and Ribaud, Y., "Preliminary Analysis of the Flow Inside a Three-Port Wave Rotor by Means of a Numerical Model," *Aerospace Science and Technology*, No. 5, 1998, pp. 289–300.
[23] Wilson, J., and Fronek, D., "Initial Results from the NASA-Lewis Wave Rotor Experiment," AIAA Paper 93–2521, Jun. 1993.
[24] Wilson, J., "An Experimental Determination of Losses in a Three-Port Wave Rotor," *Journal of Engineering for Gas Turbines and Power*, Vol. 120, Oct. 1998, pp. 833–842.
[25] Chakravarthy, S. R., and Osher, S., "A New Class of High Accuracy TVD Schemes for Hyperbolic Conservation Laws," AIAA Paper 85-0363, Jan. 1985.
[26] Anderson, W. K., Thomas, J. L., and Van Leer, B., "A Comparison of Finite Volume Flux Vector Splitting for the Euler Equations," AIAA Paper 85-0122, Jan. 1985.
[27] Jameson, A., Schmidt, W., and Turkel, E., "Numerical Solutions of the Euler Equations by Finite Volume Methods Using Runge–Kutta Time-Stepping," AIAA Paper 81-1259, Jan. 1981.
[28] Toro, E. F., *Riemann Solvers and Numerical Methods for Fluid Dynamics*, Springer, New York, 1997.

C. Tan
Associate Editor